Threshold photoelectron photoion coincidence spectroscopy and selected ion flow tube reactions of CHF$_3$: comparison of product branching ratios§

Parkes, M. A.; Chim, R. Y. L.; Mayhew, C. A.; Mikhailov, V. A.; Tuckett, R. P.

[Link to publication on Research at Birmingham portal](#)

Threshold photoelectron photoion coincidence spectroscopy and selected ion flow tube reactions of CHF$_3$: comparison of product branching ratios§

M. A. PARKES†, R. Y. L. CHIM†, C. A. MAYHEW‡, V. A. MIKHAILOV‡ and R. P. TUCKETT*†

†School of Chemistry, University of Birmingham, Edgbaston, Birmingham, B15 2TT, UK
‡School of Physics and Astronomy, University of Birmingham, Edgbaston, Birmingham, B15 2TT, UK

The threshold photoelectron and threshold photoelectron photoion coincidence spectra of CHF$_3$ in the range 13.5–24.5 eV have been recorded. Ion yields and branching ratios have been determined for the three fragments CF$_3^+$, CHF$_2^+$ and CF$^+$. The mean kinetic energy releases into fragment ions involving either C–H or C–F bond cleavage have been measured, and compared with statistical and impulsive models. CHF$_3^+$ behaves in a non-statistical manner characteristic of the small-molecule limit, with the ground electronic state and low-lying excited states of CHF$_3^+$ being largely repulsive along the C–H and C–F coordinates, respectively. The rate coefficients and product ion branching ratios have been measured at 298 K in a selected ion flow tube for the reactions of CHF$_3$ with a large number of gas-phase cations whose recombination energies span the range 6.3 through 21.6 eV. A comparison between the branching ratios from the two experiments, together with an analysis of the threshold photoelectron spectrum of CHF$_3$, shows that long-range charge transfer probably occurs for the Ar$^+$ and F$^+$ atomic ions whose recombination energies lie above *ca.* 15 eV. Below this energy, the mechanism involves a combination of short-range charge transfer and chemical reactions involving a transition state intermediate.

1. Introduction

Fluoroform (CHF$_3$) is a major industrial gas which is often used as a replacement for common feedgases, such as CHBr$_3$, CHCl$_3$ and CF$_4$, in plasma technological applications [1]. All four compounds contribute to global warming via the greenhouse effect, and CHBr$_3$ and CHCl$_3$ are serious ozone depleters in the stratosphere. The lack of Cl or Br atoms in CHF$_3$ means that it does not contribute to stratospheric ozone depletion, and the presence of one hydrogen atom means that the tropospheric lifetime of CHF$_3$ is significantly less than that of CF$_4$. The use of CHF$_3$ in plasma technology means that it is important to understand the properties of this molecule under electron and ion impact, pertinent to technological and radiofrequency plasmas, and under vacuum–UV photoexcitation with photons of similar energy. Previous work in this area includes electron impact dissociation [2, 3], electron energy loss spectroscopy [4],

vacuum–UV photoelectron spectroscopy (PES) [5–8], VUV absorption [9–11], and a positron impact dissociation study [12]. The structure of CHF$_3$ has been determined by microwave spectroscopy [13], and there have been numerous infrared and Raman studies. The interaction of CHF$_3$ with low-energy electrons has been thoroughly reviewed by Christophorou and Olthoff [14]. It is surprising, therefore, there has only been a limited amount of work done on the reaction of CHF$_3$ with gas-phase ions [1, 15–19], two of which are anion studies. There has been no measurement of the PES of CHF$_3$ under threshold conditions, no photoionization mass spectrometric study, nor a study of the fragmentation of state-selected CHF$_3^+$ using coincidence techniques. In this paper, we report a threshold photoelectron photoion coincidence (TPEPICO) study of CHF$_3$ using tunable vacuum–UV photons, complemented by a study of the reactions of CHF$_3$ with a large number of cations in a selected ion flow tube (SIFT).

An additional motivation for such studies is to understand the importance of long-range charge transfer in ion–molecule reactions. We consider the general situation of a cation (A$^+$) reacting with a neutral molecule (BC), where BC has a permanent dipole moment.

*Corresponding author. Email: r.p.tuckett@bham.ac.uk
§In honour of Professor John Simons' 70th birthday Festschrift.

Charge transfer can occur either at long range or at short range. In the long-range mechanism, A^+ and BC approach under the influence of their charge–dipole interaction, until at some critical distance (R_c) the A^+–BC and A–BC$^+$ potential energy curves cross. At this point an electron jump can take place. We have shown [20] that R_c depends on the difference in energy between the recombination energy (RE) of A^+ and the ionization energy (IE) of BC; the smaller this difference, the larger R_c. Furthermore, two important factors for a rapid electron transfer and an efficient long-range charge transfer process are a non-zero energy resonance connecting BC to an electronic state of BC$^+$ at the RE of A^+, and the transferring electron comes from a molecular orbital of BC that is not shielded from the approaching cation. So long as there is some overlap of vibrational wavefunction between BC and BC$^+$ at the RE of A^+, the evidence from similar-sized molecules (e.g. CF_4 [20], $CHClF_2$ and $CHCl_2F$ [21]) is that the magnitude of the photoionization Franck–Condon factor for BC is not as important as originally thought in determining the efficiency of such a reaction. We note that if this long-range charge transfer mechanism operates, then the branching ratios for fragmentation of $(BC^+)^{(*)}$, where (*) donates the possibility of BC$^+$ being in an excited electronic state, are expected to be independent of how this state is produced. Hence, we would expect similar product branching ratios from the ion–molecule study and from the TPEPICO photo-ionization study, assuming the photon energy in the latter experiment matches the RE of A^+ in the former.

When long-range charge transfer is unfavourable, A^+ and BC move closer together. As their separation decreases, distortion of the potential energy surface of interaction occurs. Eventually, a curve crossing can occur through which efficient charge transfer takes place. This is called short-range charge transfer. As an intermediate complex has formed, a chemical reaction, defined as the breaking and making of new bonds, may, in addition, compete with short-range charge transfer. This means that it is unlikely that the product branching ratios from the ion–molecule and from the TPEPICO experiments will mimic each other. Thus, a comparison of the fragmentation patterns from the SIFT and TPEPICO experiments, together with an analysis of the TPES of BC at the energy of the RE of A^+, may indicate which mechanism, be it long-range or short-range, is dominant for the reaction of each cation.

2. Experimental

The apparatus used for the TPEPICO study has been described in detail previously [22], the experiments being performed at the Daresbury Synchrotron Radiation Source. The coincidence experiment was performed on beamline 3.1 (1 m Seya-Namika monochromator) operating at a resolution of 0.3 nm, whilst a higher resolution threshold photoelectron spectrum (TPES) was recorded on beamline 3.2 (5 m McPherson monochromator) at a resolution of 0.15 nm. The monochromatised radiation is coupled into the interaction region and its flux is monitored via the fluorescence of a sodium salicylate coated pyrex window. Threshold photoelectrons and fragment cations from the interaction region are extracted in opposite directions by an electric field of $20 \, V \, cm^{-1}$, and are detected by a channeltron and a pair of microchannel plates, respectively. Both the threshold electron analyser and the time-of-flight mass spectrometer have been described elsewhere [22]. The raw pulses from the detectors are discriminated and are passed to a time-to-digital converter (TDC) mounted in a dedicated PC. The electrons provide a 'start' trigger while the ions provide a 'stop' signal, allowing signals from the same ionization process to be detected in coincidence.

With this apparatus, three different spectra can be recorded. Firstly, the TPES spectrum is obtained by recording the threshold electron signal as a function of photon energy. Secondly, a TPEPICO spectrum is obtained by recording the coincidence spectrum continuously as a function of photon energy. The data are recorded as a 3D map of coincidence counts versus ion time of flight versus photon energy. Sections from this map can yield either the time-of-flight mass spectrum at a defined photon energy or the yield of a particular ion. In this mode the resolution of the TOF analyser is set so that all observed fragment ions appear on one single coincidence map; in this case, spectra were recorded over 512 channels at a time resolution of 16 ns to encompass CF$^+$ through to CF_3^+. Thirdly, with a fixed photon energy, high resolution TOF spectra can be produced at the highest resolution of 8 ns. Analysis of the peak shape of the ion fragment can reveal the kinetic energy release into that ion [23, 24]. Via conservation of momentum, the mean kinetic energy release, $\langle KE \rangle_T$, into the two fragments is obtained. The ratio of $\langle KE \rangle_T$ to the energy available (E_{avail}) shows what fraction of the energy, $\langle f \rangle_T$, is channelled into translational motion of the two fragments. This value for $\langle f \rangle_T$ can be compared to statistical and impulsive models to indicate the mechanism of dissociation. These models have been reviewed elsewhere [25] and are not discussed here.

The SIFT apparatus has been described in detail elsewhere [26]. Briefly, each reagent ion of interest is produced in a high pressure electron impact ion source containing an appropriate source gas [21]. The cation is injected through a quadrupole mass filter into a flow

tube holding *ca.* 0.5 Torr of high purity (99.997%) helium as a buffer gas. The neutral reactant of choice is then admitted through an inlet at one of various points down the flow tube. The resultant ionic products are detected using a quadrupole mass spectrometer (VG SXP300). The loss of reagent ion signal, alongside the increase in the various product ion signal(s), is recorded as a function of neutral reactant concentration. The amount of neutral is altered between zero and a concentration that depletes the reactant ion signal by *ca.* 90%. Since the experiment operates under pseudo-first-order conditions with $[A^+] \ll [BC]$, and knowing the reaction length and ion flow velocity [26], a plot of the logarithm of the reagent ion signal versus neutral molecule concentration allows the rate coefficient to be determined. Rate coefficients with a upper limit of *ca.* $10^{-13} \, \mathrm{cm}^3 \, \mathrm{molecule}^{-1} \, \mathrm{s}^{-1}$ are too slow be measured in our apparatus. Percentage branching ratios for each product ion are derived from graphs of the relative product ion counts versus neutral molecule concentration, with extrapolation to zero neutral gas flow to allow for the effect of any secondary reactions. This is particularly important for reactions producing CF_3^+, since this ion reacts with CHF_3 (section 4.2). No allowance has been made in either experiment for mass discrimination effects of the respective ion detectors. This is relatively unimportant in the SIFT experiment, since the branching ratio measurements were made at the lowest possible mass resolution of the quadrupole ion detector when such effects are negligible. In the TPEPICO experiment, there is some evidence that the microchannel plate detectors discriminate in favour of lighter mass ions [27], but the difference between 51 u (CHF_2^+) and 69 u (CF_3^+), the two major product ions in this study, are relatively small. We therefore quote

a conservative error in the branching ratios of either experiment as ±10% for values greater than 10%, this error increasing for smaller branching ratios. When comparing branching ratios between the two experiments, we believe it is appropriate to propogate these errors. Therefore, agreement within *ca.* ±15% is acceptable as evidence for possible long-range charge transfer.

3. Energetics

The fragment ions observed in the dissociative photo-ionization of CHF_3 between 13 and 25 eV are CF_3^+, CHF_2^+ and CF^+ (section 4.1.2). We note that the parent ion is not observed, nor (surprisingly) fragments caused by cleavage of two bonds. The energetics of the possible photodissociation channels of CHF_3 to produce these three fragment ions are listed in table 1. The appearance energies (AE_{298}) of each fragment are measured from the first observation of signal above the background noise. For the *major* product ions, defined as a fragment formed by breaking of a single bond, the AE_{298} values (column 2) are converted into an upper limit for $\Delta_r H^{\circ}_{298}$ (column 3) for the appropriate unimolecular reaction using the procedure of Traeger and McLoughlin [28], a procedure described in detail elsewhere [29]. The vibrational frequencies of the two major fragment ions were not available in their entirety, therefore they were estimated from the isoelectronic molecules BF_3 and BHF_2. The enthalpies of formation were taken from standard reference sources [30, 31], apart from values for CF_3^+ ($406 \, \mathrm{kJ \, mol}^{-1}$) [32] and CHF_2^+ ($604 \, \mathrm{kJ \, mol}^{-1}$) [33]. For the SIFT study (table 3), apart from these standard sources, we use enthalpies of formation which are quoted in the footnote to this table.

Table 1. Thermochemistry of the observed dissociative ionization pathways of CHF_3 at 298 K.

	AE_{298}[a] (eV)	$\Delta_r H^{\circ}_{298,\mathrm{exp}}$[b] (eV)	$\Delta_r H^{\circ}_{298,\mathrm{calc}}$[c] (eV)	$AE_{298,\mathrm{calc}}$[d] (eV)
Major[e] products of CHF_3 (-697)[f]				
CF_3^+ ($+406$) + H ($+218$) + e^-	13.85 ± 0.05	13.96 ± 0.05	13.69	13.58
CHF_2^+ ($+604$) + F ($+79$) + e^-	15.03 ± 0.05	15.14 ± 0.05	14.30	14.19
Minor[g] products of CHF_3 (-697)				
CF^+ ($+1134$)[h] + HF (-273) + F ($+79$) + e^-	18.9 ± 0.2		16.97	

[a] Experimentally derived appearance energies, measured from onset of signal above noise.
[b] Experimentally measured enthalpy of reaction, derived using the method of Traeger and McLoughlin [28].
[c] Calculated value for enthalpy of reaction given by enthalpy of formation of products minus that of reactants.
[d] Calculated appearance energy at 298 K, derived using the method of Traeger and McLoughlin [28].
[e] Major products are defined as fragments caused by breaking of a single bond.
[f] Literature values for $\Delta_f H^{\circ}_{298}$ are given in $\mathrm{kJ \, mol}^{-1}$ in brackets in column 1.
[g] Minor products are defined as fragments formed by breaking of more than one bond.
[h] Note that it is not possible energetically to form CF^+ with either $F_2 + H + e^-$ or $2F + H + e^-$; $\Delta_r H^{\circ}_{298}$ is calculated to be 21.24 and 22.87 eV, respectively.

4. Results

4.1. *Photon-induced reactions of CHF₃*

4.1.1. Threshold photoelectron spectrum. The TPES of CHF_3 was recorded from 13.5–24.5 eV at a resolution of 0.15 nm (figure 1(a)). The onset of ionization is 13.85 ± 0.05 eV, in excellent agreement with Brundle *et al.* [5]. The valence molecular orbitals of CHF_3 are labelled in C_{3v} symmetry $\dots (4a_1)^2(5a_1)^2(3e)^4(4e)^4(5e)^4$ $(1a_2)^2(6a_1)^2$ [5, 14], where the numbering of the orbitals includes the carbon and fluorine 1s core orbitals. The $6a_1$ HOMO is essentially σ_{C-H} bonding, the $1a_2$, $5e$ and $4e$ orbitals are F $2p\pi$ non-bonding, $3e$ is σ_{C-F} bonding, and $5a_1$ is a mixture of σ_{C-H} and σ_{C-F} bonding in character [5]. The $4a_1$ orbital at *ca.* 24.5 eV has a small partial photoionization cross-section, and is also σ_{C-H} bonding in character [5]. The vertical ionization energies (VIE) of the first five peaks are 14.81 ($\tilde{X}\,^2A_1$), 15.57 ($\tilde{A}\,^2A_2$), 16.35 ($\tilde{B}\,^2E$), 17.28 ($\tilde{C}\,^2E$) and 20.74 ($\tilde{D}\,^2E$ and $\tilde{E}\,^2A_1$) eV, respectively. These values are in excellent agreement with previous studies using He I radiation [5–8]. At this resolution, clearly-resolved vibrational structure is only observed in the overlapped $\tilde{D}/\tilde{E}$ band at 20.74 eV, where a long progression in the ν_6 (a_1) mode, average spacing 0.056 eV or 455 cm^{-1}, can be seen. In addition, a broad band is observed centred at 19.22 eV under threshold conditions which has not been detected before. This band arises through auto-ionization of a Rydberg state of CHF_3 at the same energy, producing a threshold photoelectron. In a recent absorption study at a resolution of 0.08 nm [11], a peak is observed at 19.19 eV and assigned to the $(4a_1)^{-1}3s$ Rydberg state, whilst Wu *et al.* [9] at a slightly inferior resolution assign this peak to the $(3e \text{ or } 5a_1)^{-1}3d$ transition. In the context of interpreting the ion–molecule results (section 5), the Franck–Condon regions of the $\tilde{A}$, $\tilde{B}$ and $\tilde{C}$ states of CHF_3^+, where the electron is removed from a F $2p\pi$ non-bonding orbital of CHF_3 unshielded from the approaching cation, encompass the range *ca.* 15–18 eV. By contrast, in the range from the onset of ionization up to 15 eV and for energies greater than 18 eV, the electron is removed from a C–H or C–F σ-bonding orbital, where the fluorine atoms may cause some shielding for efficient long-range electron transfer to the approaching cation.

4.1.2. Scanning TPEPICO spectrum. A scanning-energy TPEPICO spectrum was recorded for CHF_3 from 13.5–24.5 eV with an optical resolution of 0.3 nm and a TOF resolution of 16 ns. Three fragment cations, CF_3^+, CHF_2^+ and CF^+, were observed, but the parent ion was not detected. The design of our TOF mass spectrometer means it can sometimes be difficult to
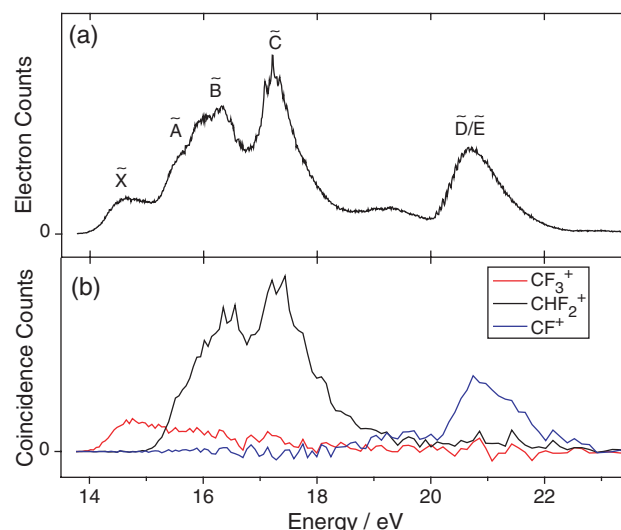

Figure 1. (a) Threshold photoelectron spectrum of CHF_3 recorded on beamline 3.2 at a resolution of 0.15 nm. (b) TPEPICO coincidence ion yields of CF_3^+, CHF_2^+ and CF^+ recorded on beamline 3.1 at a resolution of 0.3 nm.

determine the number of hydrogen atoms in a fragment ion [22]. However, with a resolution as high as 16 ns, we can state with confidence that these three fragment ions contain no contributions from CHF_3^+, CF_2^+ and CHF^+, respectively. The parent ion has never been observed unambiguously in previous electron or photon impact studies of CHF_3, although electron impact studies observe CF_2^+ and CHF^+ [2, 3]. In a recent photoion-fluorescence coincidence study of electron-impact-excited CHF_3, Furuya *et al.* [34] also observe CF_2^+ on the shoulder of the CHF_2^+ peak, but the electron energy is relatively high, 120 eV, and the presence of CF_2^+ is only determined via simulation.

Fragment ion yields abstracted from the 3D map are shown in figure 1(b). CF_3^+ is observed at the onset of ionization of CHF_3, 13.85 ± 0.05 eV, and is the only charged product produced from the ground state of CHF_3^+. The breaking of the C–H bond, and hence loss of an hydrogen atom, can be explained by the HOMO of CHF_3 being essentially σ_{C-H} bonding and the assumption that intramolecular vibrational redistribution (IVR) is slow. The appearance energy for formation of CHF_2^+ is 15.03 ± 0.05 eV, and is the major fragment produced from the $\tilde{A}$, $\tilde{B}$ and $\tilde{C}$ states of CHF_3^+. We note that these states arise from electron removal from F $2p\pi$ non-bonding orbitals so, unless IVR is now very rapid, breaking of a C–F bond is to be expected from these states. The CF^+ fragment has a weak threshold at 18.9 ± 0.2 eV which probably corresponds to production of the Rydberg state of CHF_3, with a VIE of 19.22 eV, described in section 4.1.1. The CF^+ signal then rises rapidly for $h\nu > 20$ eV, and has a maximum at 20.6 eV,

these values corresponding exactly to the adiabatic and vertical IEs of the blended $\tilde{D}\,^2E$ and $\tilde{E}\,^2A_1$ states of CHF_3^+.

These data are collected in table 1. For the CF_3^+ and CHF_2^+ fragments the appearance energies at 298 K, AE_{298} (column 2), can be converted into an upper limit of $\Delta_r H_{298,\,exp}^{\circ}$ for the appropriate unimolecular reaction (column 3) via the procedure of Traeger and McLoughlin [28]. Calculated values for $\Delta_r H_{298}^{\circ}$ are shown in column 4, and these values can be converted into calculated AE_{298} values (column 5). Comparing values for the enthalpies of reaction, $CHF_3 \rightarrow CF_3^+ + H + e^-$ is 0.27 eV more endothermic than the calculated value. Thus the onset of CF_3^+ does not relate to its thermochemical threshold, but to the energy of the ground state of CHF_3^+ which is probably repulsive along the dissociative C–H coordinate. The same argument holds true for the production of $CHF_2^+ + F + e^-$ where the difference in endothermicities in now larger, 0.84 eV. Thus the $\tilde{A}$, $\tilde{B}$ and $\tilde{C}$ states of CHF_3^+ are probably repulsive along the C–F coordinate, and dissociate state-selectively to $CHF_2^+ + F$. CHF_3^+ is therefore behaving non-statistically in the small-molecule limit [22]. The method of converting AE_{298} into an upper limit of $\Delta_r H_{298,\,exp}^{\circ}$ is not appropriate for fragment ions in which more than one bond breaks. With this proviso, we comment that the onset of CF^+ at 18.9 eV lies *ca.* 2 eV above its corresponding calculated threshold, noting that on energetic grounds CF^+ can only form with $HF + F$ as accompanying neutral partners. It appears that CF^+ relates to state-selected dissociation of both the autoionising Rydberg state of CHF_3 at 19.22 eV and to the $\tilde{D}$ and $\tilde{E}$ states of the parent ion.

4.1.3. Fixed energy TPEPICO spectra. Fixed energy spectra were recorded with a TOF resolution of 8 ns for CF_3^+ at 14.76 eV and for CHF_2^+ at 16.35 and 17.36 eV, representing the VIEs of the $\tilde{X}$, $\tilde{B}$ and $\tilde{C}$ states of CHF_3^+, respectively. Mean translational kinetic energy releases, $\langle KE \rangle_T$, were obtained from each of these spectra as described elsewhere [23, 24]. Briefly, for each TPEPICO-TOF spectrum a small basis set of peaks, each with a discrete energy release ε_t is computed, and assigned a probability. The discrete energies are given by $\varepsilon_t(n) = (2n-1)^2 \Delta E$, where $n = 1, 2, 3, 4 \ldots$. ΔE depends on the statistical quality of the data; the higher the signal-to-noise ratio, the lower ΔE and the higher n can be set to obtain the best fit. Each computed peak in the kinetic energy release distribution spans the range $4(n-1)^2 \Delta E$ to $4n^2 \Delta E$, centred at $\varepsilon_t(n) + \Delta E$. The reduced probability of each discrete energy, $P(\varepsilon_t)$, is varied by linear regression to minimise the least-squared errors between the simulated and experimental
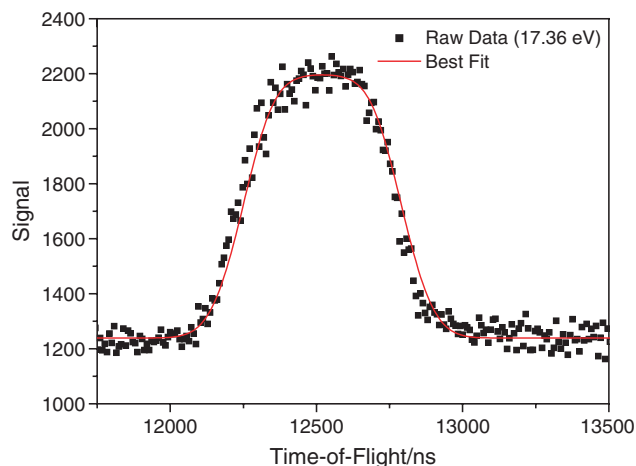

Figure 2. Time-of-flight spectrum (dots) for the CHF_2^+ fragment ion produced from dissociative photoionization of CHF_3 at a photon energy of 17.36 eV. The solid line is the best fit, using the procedure described elsewhere [23, 24]. The total, average translational kinetic energy release, $\langle KE \rangle_T$, is determined to be 1.18 ± 0.03 eV, corresponding to 37% of the available energy.

TOF peak. From the basis set of ε_t and $P(\varepsilon_t)$, $\langle KE \rangle_T$ is easily determined. The analysis can accommodate a range of isotopes in the daughter ion, but this facility is clearly not needed in this CHF_3^+ project.

Figure 2 shows the TOF spectrum for CHF_2^+ at 17.36 eV, the fit to the data, and the agreement is excellent. Table 2 lists the experimental $\langle KE \rangle_T$ and $\langle f \rangle_T$ values, as well as the calculated impulsive and statistical $\langle f \rangle_T$ values. Without overinterpreting this data, there is clear indication that the $\tilde{B}$ and $\tilde{C}$ states of CHF_3^+ dissociate non-statistically by cleavage of a C–F bond, with a value for $\langle f \rangle_T$ close to the dynamical, impulsive limit. The ground state of CHF_3^+ also seems to dissociate by C–H bond cleavage via a mechanism that has a significant impulsive component. Both these observations are consistent with the yield data for these two ions described in section 4.1.2.

4.2. Bimolecular cation-induced reactions of CHF₃

4.2.1. Rate coefficients. Reactions between a series of ions, with a range of recombination energies (RE) from 6.27–21.56 eV, with CHF_3 were studied using the SIFT technique. For each reaction a second order rate coefficient, k_{exp}, was measured, and a value calculated, k_{calc}, using modified-average dipole orientation (MADO) theory [35]. This theory is based on the classical Langevin model [36, 37] plus a contribution from the permanent dipole moment of CHF_3. To calculate the MADO rate coefficient, values for both the dipole moment (1.65 D) and the

Table 2. Total mean kinetic energy releases $\langle KE \rangle_T$ of for the two-body fragmentation of valence states of CHF_3.

Electronic state of parent ion	Daughter ion	$h\nu$/eV	E_{avail}/eV[a]	$\langle KE \rangle_t$/eV	$\langle f \rangle_T$ Experimental[b]	$\langle f \rangle_T$ Statistical	$\langle f \rangle_T$ Impulsive
$CHF_3^+ \tilde{X}^2A_1$	$C_TF_3^+$	14.76	1.24	0.66 (9)	0.53	0.10	0.94
$\tilde{B}^2E$	CHF_2^+	16.35	2.22	1.02 (4)	0.46	0.10	0.53
$\tilde{C}^2E$	CHF_2^+	17.36	3.23	1.18 (3)	0.37	0.10	0.53

[a] $E_{avail} = h\nu +$ thermal energy of parent molecule at 298 K (0.06 eV) $- AE_{298,calc}$. See text.
[b] Given by $\langle KE \rangle_T / E_{avail}$.

polarizability volume ($3.15 \times 10^{-30}\,m^3$) of CHF_3 were required [14]. Data for k_{exp} and k_{calc} is shown in column 2 of table 3. The efficiency of the reaction is defined as k_{exp}/k_{calc}.

For those cations whose RE is above the IE (CHF_3), 13.85 eV, k_{exp} is very similar to k_{calc}, implying that these are efficient reactions which occur upon nearly every collision. The one exception is Kr^+ (RE = 14.00 eV), just above the IE (CHF_3), where the efficiency is only 0.5. There is no obvious correlation between efficiency of reaction and RE of the cation. For cations with RE below the IE (CHF_3), only seven of the seventeen collision systems studied exhibited any reactivity. Of these seven, all but O^+ and OH^+ have k_{exp} which is somewhat lower than k_{calc}, and for CO_2^+ and CF_3^+ the reaction efficiency falls to *ca.* 0.25. Energetics alone cannot explain the observed values of k_{exp}. For example, O^+ and CO_2^+ differ in RE by only 0.16 eV, yet the former reacts with unity efficiency whereas the latter has an efficiency less than 0.25. This suggests that steric effects for this group of reactions may be important. Such reactions can only occur via a short-range intermediate (section 1), so it is not surprising that such effects may play an important role.

4.2.2. Branching ratios. The branching ratios of the product cations are also measured in the SIFT experiment, data shown in column 3 of table 3. We note that the resolution of the quadrupole mass spectrometer, when used for product ion assignment, is better than 1 u, therefore there can be no ambiguity in the assignment of product cations. The parent ion, CHF_3^+, is not observed, and the three major product ions are CF_3^+, CHF_2^+ and CF^+. The two exceptions are that the reaction of H_2O^+ (RE = 12.56 eV) produces exclusively CF_2OH^+, and there is a small yield of CF_2^+ (15%) for the reaction of Ne^+, the ion with highest RE, 21.56 eV, studied. Thus the SIFT and TPEPICO experiments detect predominantly the same cationic products.

Columns 4 and 5 of table 3 present proposed neutral products and associated enthalpies of reaction at 298 K. The proposed pathways are those which are both chemically feasible and are the most exothermic.

For nearly all the reactions studied, there is an exothermic pathway, consistent with an experimental rate coefficient within an order of magnitude of k_{calc}. The one exception is the relatively slow reaction of CO_2^+ with CHF_3 producing CHF_2^+ (55%), where both possible neutral channels (FOCO and $F + CO_2$) are mildly endothermic. Previous work has highlighted how entropic effects can drive reactions which are enthalpically unfavourable [40], and we note that only a relatively small value for $\Delta_r S^{\circ}_{298}$ (*ca.* 30 J mol^{-1}K^{-1}) would be needed to overcome the endothermicity of the former channel. It should also be noted that, ignoring any entropic effects, the reaction of Kr^+ with CHF_3 to produce the minor product, CHF_2^+ (16%), is only exothermic for Kr^+ in its excited $^2P_{1/2}$ spin–orbit state.

Two further points can be made. First, the cations CF_x^+ ($x = 1$–3) all react with CHF_3^+ with efficiencies between *ca.* 0.3–0.8, despite all having a RE less than IE (CHF_3). The only product cation for all three reactions is CHF_2^+, and therefore F^- transfer from CHF_3 to produce neutral CF_{x+1} is the driving force. Second, a comparison between the products from the Kr^+ $^2P_{3/2}$ (RE = 14.00 eV) and CO^+ (RE = 14.01 eV) reactions is revealing. Both cations have REs greater than IE (CHF_3), with both reactions having relatively high efficiency. Yet the ratio of the products CHF_2^+ and CF_3^+ changes from 0.2 for Kr^+ to 32 for CO^+. This point is discussed further in section 5.

There have been relatively few studies of the reactivity of CHF_3 with positive ions, and very surprisingly none, to our knowledge, in a selected ion flow tube. The reaction of CF_3^+ with CHF_3 has been studied using a crossed beam electrostatic trapping cell at a range of collision energies [1], the rate coefficient was not measured but the ionic products were. Our results do not agree, as Peko *et al.* observe the products CF^+, CF_3^+ and CHF_2^+, whereas we observe only CHF_2^+. The discrepancy may be due to the high collisional energy used in their study. Pabst *et al.* [15] studied the reaction of CHF_3 with fragment ions produced from electron impact ionization of CHF_3 under relatively high pressure conditions. They observed the same fragments

Table 3. Rate coefficients at 298 K, product cations and branching ratios, and suggested neutral products[a] for reactions of gas-phase cations with CHF_3. The calculated enthalpy of reaction at 298 K is shown in the fifth column.

Reagent ion (RE^b/eV)	Rate coefficient[c]/ $10^{-9} \, cm^3 \, molecule^{-1} \, s^{-1}$	Product ions (%)	Proposed neutral products	$\Delta_r H^{\circ}_{298}$ /kJ mol^{-1}
H_3O^+ (6.27)	– [2.3]	No reaction[d]	–	–
SF_3^+ (8.32)	– [1.4]	No reaction	–	–
CF_3^+ (9.04)	0.4 [1.5]	CHF_2^+ (100)	CF_4	−38
CF^+ (9.11)	1.3 [1.9]	CHF_2^+ (100)	CF_2	−15
NO^+ (9.26)	– [2.0]	No reaction	–	–
SF_5^+ (9.78)	– [1.3]	No reaction	–	–
SF_2^+ (10.24)	– [1.5]	No reaction	–	–
SF^+ (10.31)	– [1.7]	No Reaction	–	–
CF_2^+ (11.44)	1.4 [1.7]	CHF_2^+ (100)	CF_3	−87
SF_4^+ (11.99)	– [1.4]	No reaction	–	–
O_2^+ (12.07)	– [1.9]	No reaction	–	–
Xe^+ (12.13)	– [1.3]	No reaction	–	–
H_2O^+ (12.62)	1.5 [2.4]	CF_2OH^+ (100)	$HF + H$	−102
N_2O^+ (12.89)	– [1.7]	No reaction	–	–
OH^+ (13.25)	2.2 [2.4]	CHF_2^+ (68)[e]	HOF	−90
			$HF + O$	−15
		CF_3^+ (32)[e]	H_2O	−432
O^+ (13.62)	2.5 [2.4]	CHF_2^+ (100)	OF	−153
CO_2^+ (13.76)	0.4 [1.7]	CHF_2^+ (55)	FOCO	10
		CF_3^+ (45)	HOCO	−11
			or $CO_2 + H$	−8
Kr^+ (14.00 (& 14.67)[f])	0.8 [1.5]	CHF_2^+ (16)	$Kr + F$	30 (or −35)[f]
		CF_3^+ (84)	$Kr + H$	−30 (or −95)[f]
CO^+ (14.01)	2.0 [2.0]	CHF_2^+ (97)	$CO + F$	29
			or FCO	−112
		CF_3^+ (3)	$CO + H$	−30
			or HCO	−95
N^+ (14.53)	2.3 [2.6]	CHF_2^+ (61)	$N + F$	−22
			or NF	−96
		CF_3^+ (39)	$N + H$	−81
			or NH	−395
N_2^+ (15.58)	2.1 [2.0]	CHF_2^+ (46)	$N_2 + F$	−123
		CF_3^+ (54)	$N_2 + H$	−182
Ar^+ (15.76)	1.8 [1.8]	CHF_2^+ (72)	$Ar + F$	−141
		CF_3^+ (28)	$Ar + H$	−200
F^+ (17.42)	1.9 [2.3]	CHF_2^+ (100)	$F + F$	−300
			or F_2	−459

(*Continued*)

Table 3. Continued.

Reagent ion (RE[b]/eV)	Rate coefficient[c]/ 10^9 cm^3 molecule^{-1} s^{-1}	Product ions (%)	Proposed neutral products	$\Delta_r H^\circ_{298}$ /kJ mol^{-1}
Ne$^+$ (21.56)	1.9 [2.2]	CHF$_2^+$ (7) CF$_2^+$ (15) CF$^+$ (78)	Ne + F Ne + HF Ne + HF + F	−700 −734 −442

[a] The majority of the enthalpies of formation at 298 K for ion and neutral species are taken from standard sources [30, 31]. Exceptions are more recent experimental values for CF$_3$, CF$_3^+$ [32], and CHF$_2^+$ [33]. For neutral FOCO and HOCO, we use experimental and *ab initio* values, respectively, for their lower *trans* isomer of −356 and −179 kJ mol^{-1} [38, 39].
[b] Recombination energy (RE) of reactant ion. For molecular ions, the RE is given for $v = 0$. For atomic ions, the RE is given for the lower spin-orbit component, where appropriate. The one exception is Kr$^+$ where the RE is given for both $^2P_{3/2}$ and $^2P_{1/2}$ components (see text)
[c] The values in square brackets are calculated by the Modified Average Dipole Orientation model [35], using literature values for the dipole moment (1.65 D) and polarizability volume (3.15×10^{-30} m^3) of CHF$_3$ [14].
[d] No reaction means the rate coefficient is less than *ca.* 10^{-13} cm^3 molecule^{-1} s^{-1}.
[e] There is also a trace (< 1%) of product with mass 87 u, OH$\cdots$CHF$_3^+$, from this reaction.
[f] Values in brackets refer to Kr$^+$ in its excited spin-orbit state.

from electron impact as we observe from our photon-induced study (section 4.1), but in addition they observed CF$_2^+$, F$^+$ and the parent ion. However, these three ions occurred only as very small percentage yields, especially CHF$_3^+$ (0.5%). We note that the ions in the study of Pabst *et al.* were generated at high electron impact energies of 150–200 eV, compared to photon energies of 13–25 eV in our TPEPICO study. The rates of the reactions of CF$_3^+$ and F$^+$ with CHF$_3$ are in fairly good agreement with our measurements, but their rates for the reaction of CF$_2^+$ and CF$^+$ with CHF$_3$ are much lower. Chau and Bowers [16] used the ion cyclotron resonance technique to study the reactions of CHF$_3$ with the rare gas ions and N$_2^+$, CO$^+$, CO$_2^+$ and N$_2$O$^+$. They were unable to measure product distributions but commented that charge transfer dominates over chemical reaction channels. The majority of the rates they measured are in good agreement to ours. Jiao *et al.* [17] used Fourier transform mass spectrometry to study the reactions of Ar$^+$, CF$_2^+$ and CF$_3^+$ with CHF$_3$. They measure rate coefficients which are much lower than ours, but their product yields are similar.

5. Comparison between TPEPICO and SIFT data

Figure 3 shows the branching ratios from the TPEPICO and SIFT studies as a function of energy. The former appear as continuous graphs, whereas the latter appear as data points at defined RE values of the ions. As described in section 1, a comparison of the branching ratios may indicate the mechanism in operation for the cation reactions. Only seven out of the twenty four ions studied have REs greater than IE (CHF$_3$), so it is only for these seven reactions that long-range charge transfer
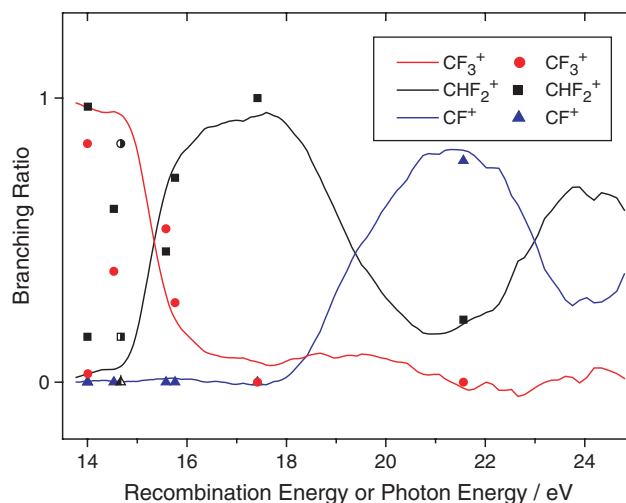

Figure 3. Comparison of the ionic products from ion–molecule studies of CHF$_3$ with TPEPICO photoionization branching ratios over the energy range 14–25 eV. The half-filled symbols at 14.67 eV correspond to Kr$^+$ in its excited $^2P_{1/2}$ spin–orbit component.

is possible. Of these seven ions, the four with RE > 15 eV show differing behaviour when comparing branching ratios to the photon-induced study. For Ar$^+$, F$^+$ and Ne$^+$ the agreement between data from the two experiments is particularly good, well within the 15% error that we discussed in section 2 as acceptable evidence for long-range charge transfer. For N$_2^+$ there is a significant difference, a ratio of 48% CHF$_2^+$ to 52% CF$_3^+$ in the ion–molecule reaction to be compared with 68% CHF$_2^+$ to 32% CF$_3^+$ in the TPEPICO experiment at a photon energy of 15.58 eV. For N$_2^+$, Ar$^+$ and F$^+$ there is a significant Franck–Condon intensity in the TPES (figure 1(a)) at the RE of these three ions and the electron is removed from an unshielded F 2pπ

molecular orbital, whereas at the RE of Ne^+, 21.56 eV, the Franck–Condon activity is low and the electron is removed from a mixture of σ_{C-H} and σ_{C-F} shielded orbitals.

In section 1, we described experiments [20, 21] that suggested that an energy resonance and the transfer of an unshielded electron were sufficient criteria for long-range charge transfer to occur; an appreciable Franck–Condon vibrational overlap factor between $BC_{v=0}$ and $(BC^+)^{(*)}{}_{v'}$ was not necessary. The evidence from these reactions with CHF_3 is not so clear. For N_2^+, despite all three criteria being satisfied, the branching ratio agreement is poor, suggesting that long-range charge transfer may not be the dominant mechanism. For Ar^+ all three criteria are satisfied, and the agreement between branching ratios is excellent; long-range charge transfer is apparently dominant. We note that, despite only a small difference between the RE of N_2^+ and Ar^+, 0.18 eV, the branching ratios from the two SIFT experiments are very different. We are unable to explain this surprising result, other than state the obvious that N_2^+ is molecular whereas Ar^+ is atomic. For F^+, there is a small discrepancy between the branching ratios of the two experiments, in that CHF_2^+ (100%) is the only observed product ion, whereas the TPEPICO experiment at 17.42 eV photon energy produces CHF_2^+ (93%) and CF_3^+ (7%). However, the F^+ signal was very weak, and it is possible that we did not have the sensitivity to observe the CF_3^+ channel. It seems likely that long-range charge transfer is dominant. For Ne^+, the RE of 21.56 eV corresponds to the very edge of the Franck–Condon region of the $\tilde{D}/\tilde{E}$ states of CHF_3^+, and the electron is removed from a shielded orbital. Despite the excellent agreement between the branching ratio data, therefore, we suggest that Ne^+ charges transfers with CHF_3 via a short-range intermediate. We note, however, that any judgements on how good agreement between branching ratios needs to be and what constitutes an appreciable Franck–Condon factor are subjective. We have imposed, somewhat arbitrarily, an agreement within 15% in the branching ratios as evidence for long-range charge transfer, whilst the detection of an energy resonance with very low Franck–Condon factor depends upon the sensitivity of the electron analyser.

For the three ions with RE in the range 13.9–15.0 (Kr^+, CO^+ and N^+), there is significantly poorer agreement between the branching ratios from the two experiments. Indeed, for CO^+ there is total disagreement in that the bimolecular chemical reaction produces CHF_2^+ (97%) as its main product whereas the photon-induced reaction produces CF_3^+ (*ca.* 90%). The agreement of the branching ratios for N^+

(RE = 14.53 eV) is poor, the discrepancy for CF_3^+ and CHF_2^+ yields being greater than a factor of 2. Thus for CO^+ and N^+ long-range charge transfer cannot be the preferred reaction mechanism. We note that in each case the electron would have to transfer from the highest occupied molecular orbital of CHF_3, a σ_{C-H} bonding orbital which will be shielded by three bulky fluorine atoms. The data points for Kr^+ are in better agreement, within 10–15% of the photon-induced branching ratios, this being true at the energies of both of its spin–orbit components, $^2P_{3/2}$ at 14.00 and $^2P_{1/2}$ at 14.67 eV. As stated earlier, CHF_2^+ (16%), only becomes energetically allowed if Kr^+ exists in its excited spin–orbit state (table 3). Unfortunately, we are unable to determine how thermalized Kr^+ is in the SIFT apparatus.

6. Conclusions

The threshold photoelectron and threshold photoelectron photoion coincidence spectrum of CHF_3 in the range 13.5–24.5 eV have been recorded. Ion yields and branching ratios have been determined for the three fragments produced. No parent ion has been observed, the lowest-energy fragment is CF_3^+, and as the photon energy increases first CHF_2^+ and then CF^+ are formed. The mean kinetic energy releases into fragment ions involving one bond cleavage have been measured and compared with statistical and impulsive models. Our work has shown that CHF_3^+ behaves in a non-statistical manner characteristic of the small-molecule limit, with the ground state and low-lying excited states of CHF_3^+ being largely repulsive along the C–H and C–F coordinates, respectively. The rate coefficients and branching ratios have been measured at 298 K for the reactions of CHF_3 with H_3O^+, CF_n^+ ($n = 1–3$), SF_x^+ ($x = 1–5$), NO^+, O_2^+, Xe^+, H_2O^+, N_2O^+, OH^+, O^+, CO_2^+, Kr^+, CO^+, N^+, N_2^+, Ar^+, F^+ and Ne^+. Comparison with theory shows that for reactions where charge transfer is exothermic, i.e. RE (ion) > IE (CHF_3), most of the reactions occur efficiently, i.e. $k_{exp} \approx k_{calc}$. For reactions at lower energies, the efficiency can be significantly reduced. Comparisons between TPEPICO and SIFT branching ratios, together with an analysis of the TPES of CHF_3, show that long-range charge transfer probably occurs for the Ar^+ and F^+ atomic ions with recombination energies above *ca.* 15 eV. The importance or otherwise of an appreciable Franck–Condon factor for the neutral molecule, CHF_3, at the RE of the ion is unclear. Below 15 eV, a combination of short-range charge transfer and chemical reactions take place.

References

[1] B.L. Peko, R.L. Champion, M.V.V.S. Rao, J.K. Olthoff. *J. Appl. Phys.*, **92**, 1657 (2002).
[2] I. Torres, R. Martínez, F. Castaño. *J. Phys.* B, **35**, 2423 (2002).
[3] M. Goto, K. Nakamura, H. Toyodo, H. Sugai. *Jpn. J. Appl. Phys.*, **33**, 3602 (1994).
[4] J.F. Ying, K.T. Leung. *Phys. Rev.* A, **53**, 1476 (1995).
[5] C.R. Brundle, M.B. Robin, H. Basch. *J. chem. Phys.*, **53**, 2196 (1970).
[6] B.P. Pullen, T.A. Carlson, W.E. Moddeman, G.K. Schweitzer, W.E. Bull, F.A. Grimm. *J. chem. Phys.*, **53**, 768 (1970).
[7] A.W. Potts, H.J. Lempka, D.G. Streets, W.C. Price. *Phil. Trans. R. Soc.* A, **268**, 59 (1970).
[8] T.A. Carlson, R.M. White. *Faraday Dissc. Chem. Soc.*, **54**, 104 (1972).
[9] C.Y.R. Wu, L.C. Lee, D.L. Judge. *J. chem. Phys.*, **71**, 5221 (1979).
[10] P. Sauvageau, R. Gilbert, P.P. Berlow, C. Sandorfy. *J. chem. Phys.*, **59**, 762 (1979).
[11] S. Ali, R.P. Tuckett. in preparation (2005).
[12] J. Moxom, D.M. Schrader, G. Laricchia, J. Xu, L.D. Hulett. *Phys. Rev.* A, **62**, 52708 (2000).
[13] G. Gazzoli, L. Cludi, G. Cotti, L. Dore, C. Degli Esposti, M. Bellini, P. de Natale. *J. Molec. Spec.*, **163**, 521 (1994).
[14] L.G. Christophorou, J.K. Olthoff. *Fundamental Electron Interactions with Plasma Processing Gases*, Kluwer Academic/Plenum Publishers, New York (2004).
[15] M.J.K. Pabst, H.S. Tan, J.L. Franklin. *Int. J. Mass Spec. Ion Phys.*, **20**, 191 (1975).
[16] M. Chau, M.T. Bowers. *Int. J. Mass Spec. Ion Phys.*, **24**, 191 (1977).
[17] C.Q. Jiao, R. Nagpal, P.D. Haaland. *Chem. Phys. Lett.*, **269**, 117 (1997).
[18] C.A. Mayhew, R. Peverall, C.M. Timperley, P. Watts. *Int. J. Mass Spectrom.*, **233**, 155 (2004).
[19] R. Peverall, R.A. Kennedy, C.A. Mayhew, P. Watts. *Int. J. Mass Spec. Ion Phys.*, **171**, 51 (1997).
[20] G.K. Jarvis, R.A. Kennedy, C.A. Mayhew, R.P. Tuckett. *Int. J. Mass Spectrom.*, **202**, 323 (2000).
[21] C.R. Howle, C.A. Mayhew, R.P. Tuckett. *J. phys. Chem.* A, **109**, 3626 (2005).
[22] P.A. Hatherly, D.M. Smith, R.P. Tuckett. *Zeit. Phys. Chem.*, **195**, 97 (1996).
[23] I. Powis, P.I. Mansell, C.J. Danby. *Int. J. Mass Spectrom. Ion Phys.*, **32**, 15 (1979).
[24] G.K. Jarvis, D.P. Seccombe, R.P. Tuckett. *Chem. Phys. Lett.*, **315**, 287 (1999).
[25] C.R. Howle, D.J. Collins, R.P. Tuckett, A.E.R. Malins. *Phys. Chem. Chem. Phys.*, **7**, 2287 (2005).
[26] D. Smith, N.G. Adams. *Adv. At. Molec. Phys.*, **24**, 1 (1988).
[27] G.K. Jarvis, K.J. Boyle, C.A. Mayhew, R.P. Tuckett. *J. Phys. Chem.* A, **102**, 3219 (1998).
[28] J.C. Traeger, R.G. McLoughlin. *J. Am. Chem. Soc.*, **103**, 3647 (1981).
[29] W. Zhou, D.J. Collins, R.Y.L. Chim, D.P. Seccombe, R.P. Tuckett. *Phys. Chem. Chem. Phys.*, **6**, 3081 (2004).
[30] M.W. Chase. *J. phys. Chem. Ref. Data*, monograph no. 9, webbook.nist.gov/chemistry (1998).
[31] S.G. Lias, J.E. Bartmess, J.F. Lebman, J.L. Holmes, R.D. Levin, W.G. Mallard. *J. Phys. Chem. Ref. Data*, **17**, supplement no. 1 (1988).
[32] G.A. Garcia, P.M. Guyon, I. Powis. *J. phys. Chem.* A, **105**, 8296 (2001).
[33] W. Zhou, D.P. Seccombe, R.P. Tuckett, M.K. Thomas. *Chem. Phys.*, **283**, 419 (2002).
[34] K. Furuya, K. Matsuo, K. Maruyama, Y. Hatano, T. Ogawa. *J. Phys.* B, **35**, 1015 (2002).
[35] T. Su, W.J. Chesnavich. *J. Chem. Phys.*, **76**, 5183 (1982).
[36] P.M. Langevin. *Ann. Chim. Phys.*, **5**, 245 (1905).
[37] G. Gioumousis, D.P. Stevenson. *J. chem. Phys.*, **29**, 294 (1958).
[38] D.W. Arnold, S.E. Bradforth, E.H. Kim, D.M. Neumark. *J. Chem. Phys.*, **102**, 3493 (1995).
[39] T.V. Duncan, C.E. Miller. *J. chem. Phys.*, **113**, 5138 (2000).
[40] K.K. Irikura. *J. Am. Chem. Soc.*, **121**, 7689 (1999).